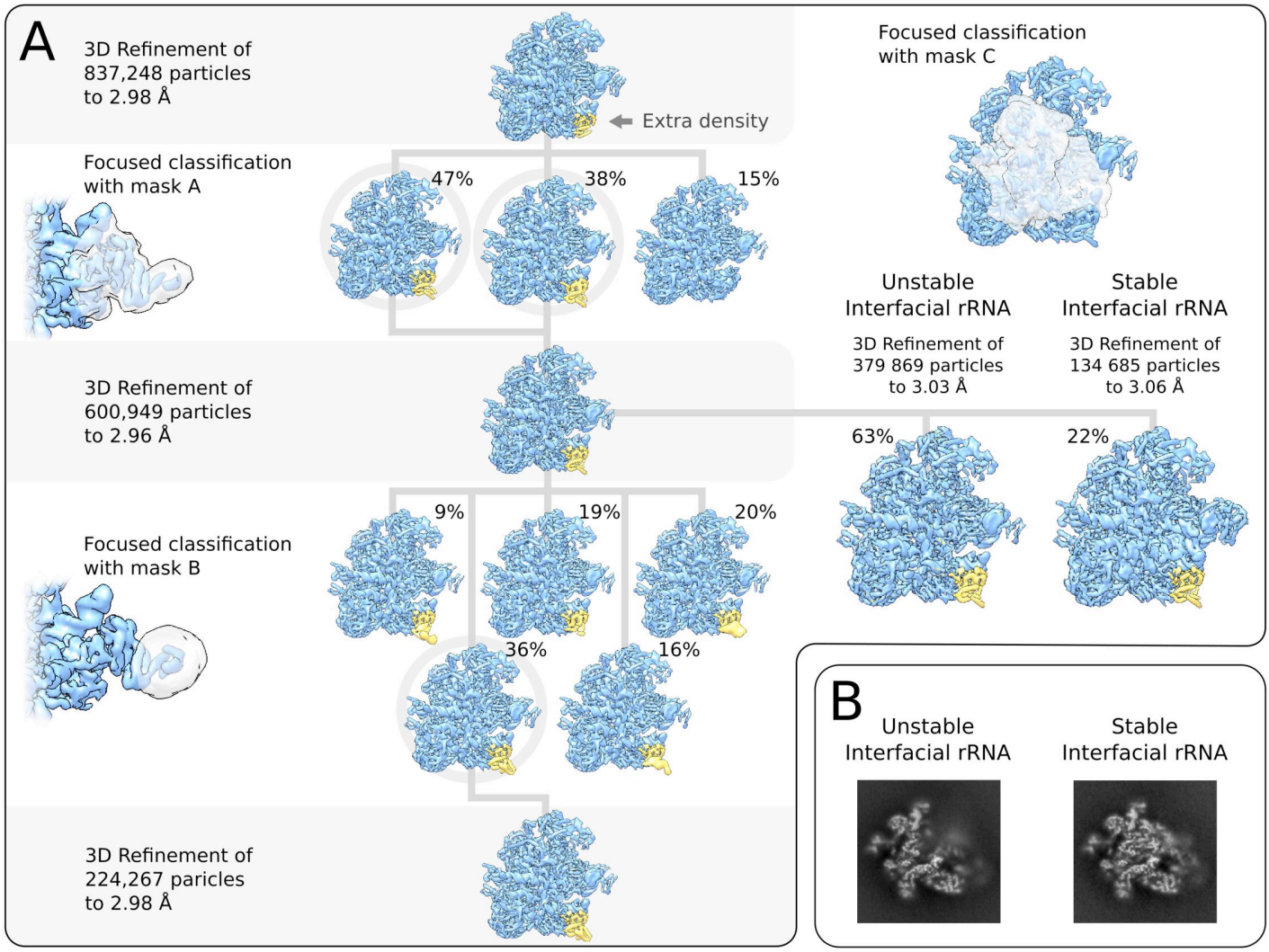

Supplementary Figure 1

EM data processing pipeline for dataset 2.

Initial processing focused on isolating particles with extraneous density by applying a mask over the MALSU1–L0R8F8–mt-ACP module (mask A). The density for this region was further improved by applying a mask over the density for just L0R8F8–mt-ACP (mask B). The particles were separated into two subclasses based on the stability of mt-rRNA using a mask over the interfacial mt-rRNA (mask C). These classes were used for model building and interpretation. Mitoribosomes are viewed as in Fig. 1B, with density corresponding to the MALSU1–L0R8F8–mt-ACP module in yellow. Masks are shown in white. (**B**) Slices through the 3D projections for both assembly intermediates. Nebulous density at the intersubunit interface for the map with "unstable" interfacial mt-rRNA suggests that the mt-rRNA is present, but adopts multiple conformations.

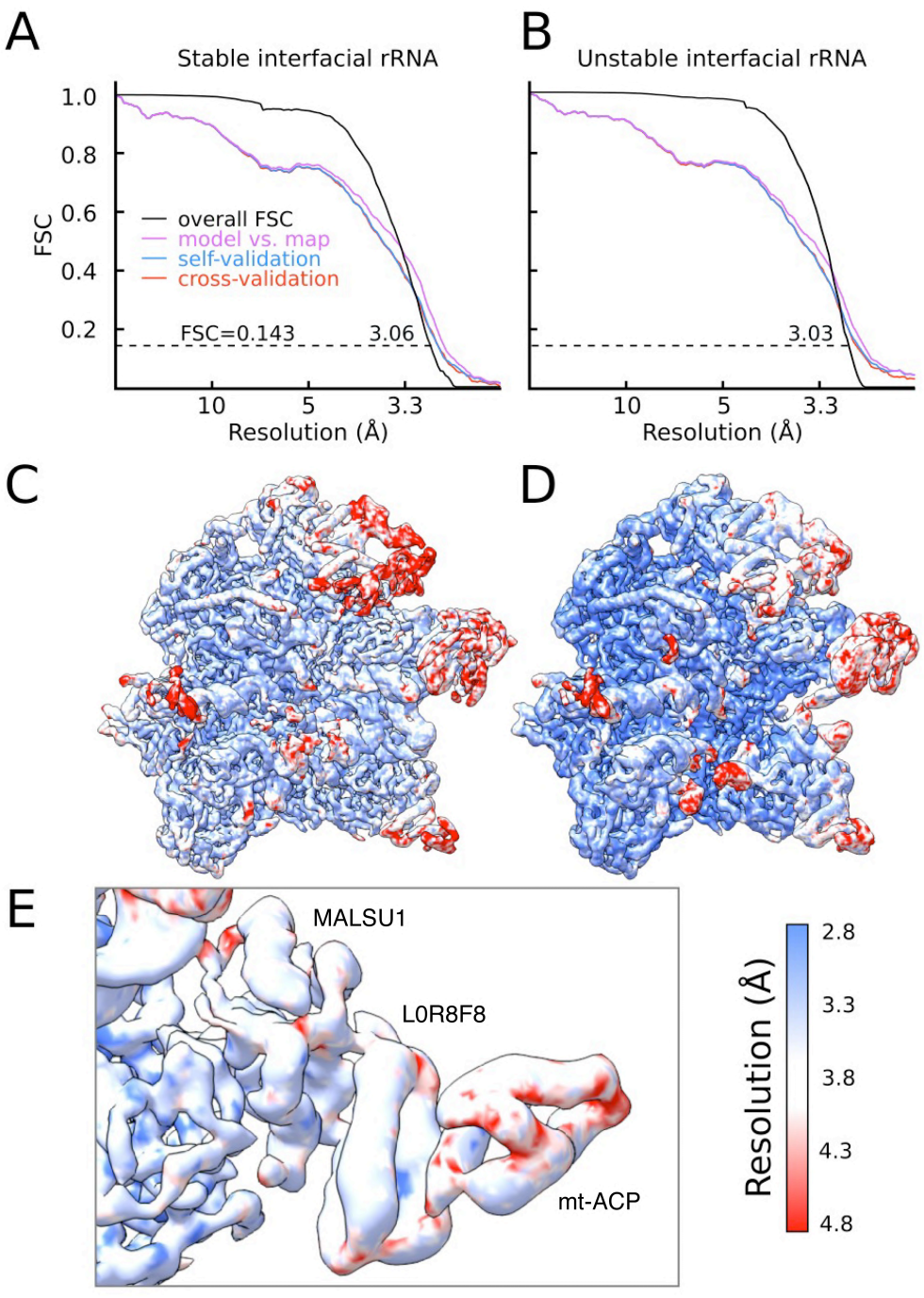

Supplementary Figure 2

Map quality.

(**A**) Fourier shell correlation (FSC) curves for the two mt-LSU assembly intermediates, with and without folded interfacial mt-rRNA. Also plotted are the FSC curves calculated between the refined model and final map, and the self and cross-validated correlations. The nominal resolution estimated from the map-to-map correlation at FSC = 0.143 is reported and agrees well with the model-to-map correlation at FSC = 0.5. (**B**) The cryo-EM map for each assembly intermediate colored by local resolution.

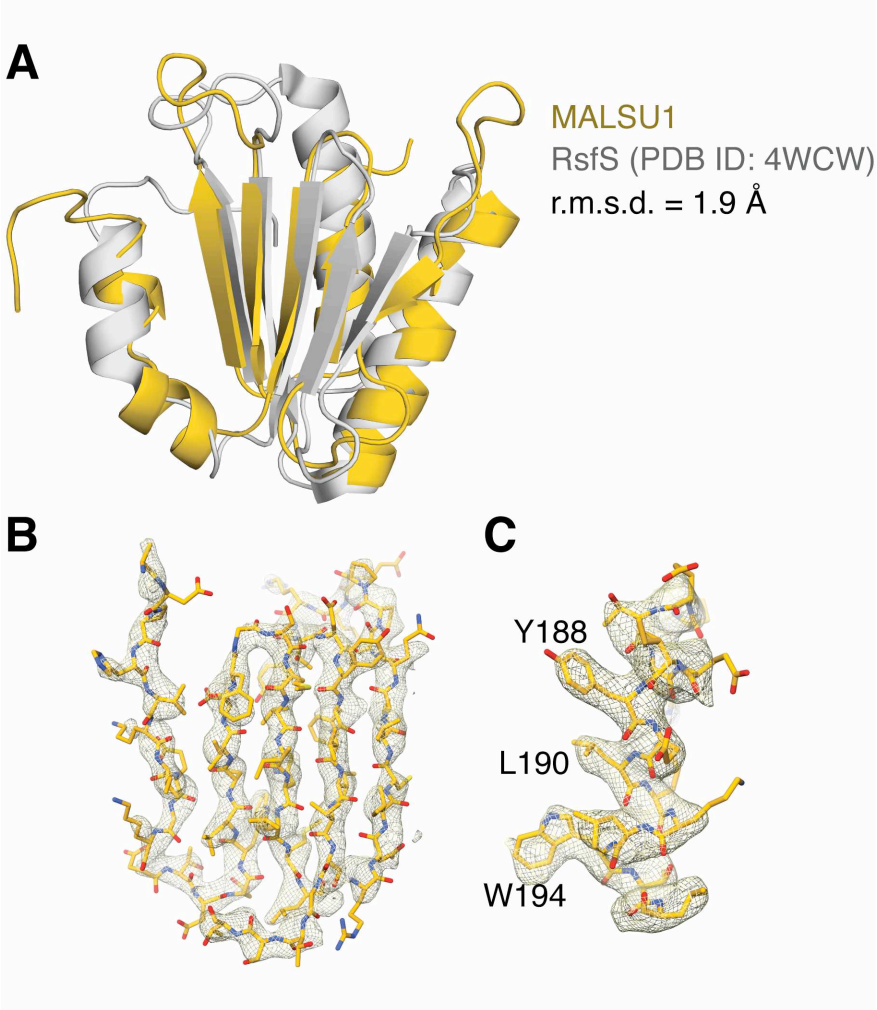

Supplementary Figure 3

Identification of MALSU1.

(**A**) Superposition of MALSU1 with RsfS from *Mycobacterium tuberculosis* (PDB ID: 4WCW). (**B**) Fit of the model for the 5-stranded β-sheet of MALSU1 to the map. (**C**) Density and model for an α-helix of MALSU1 demonstrating the quality of side-chain density.

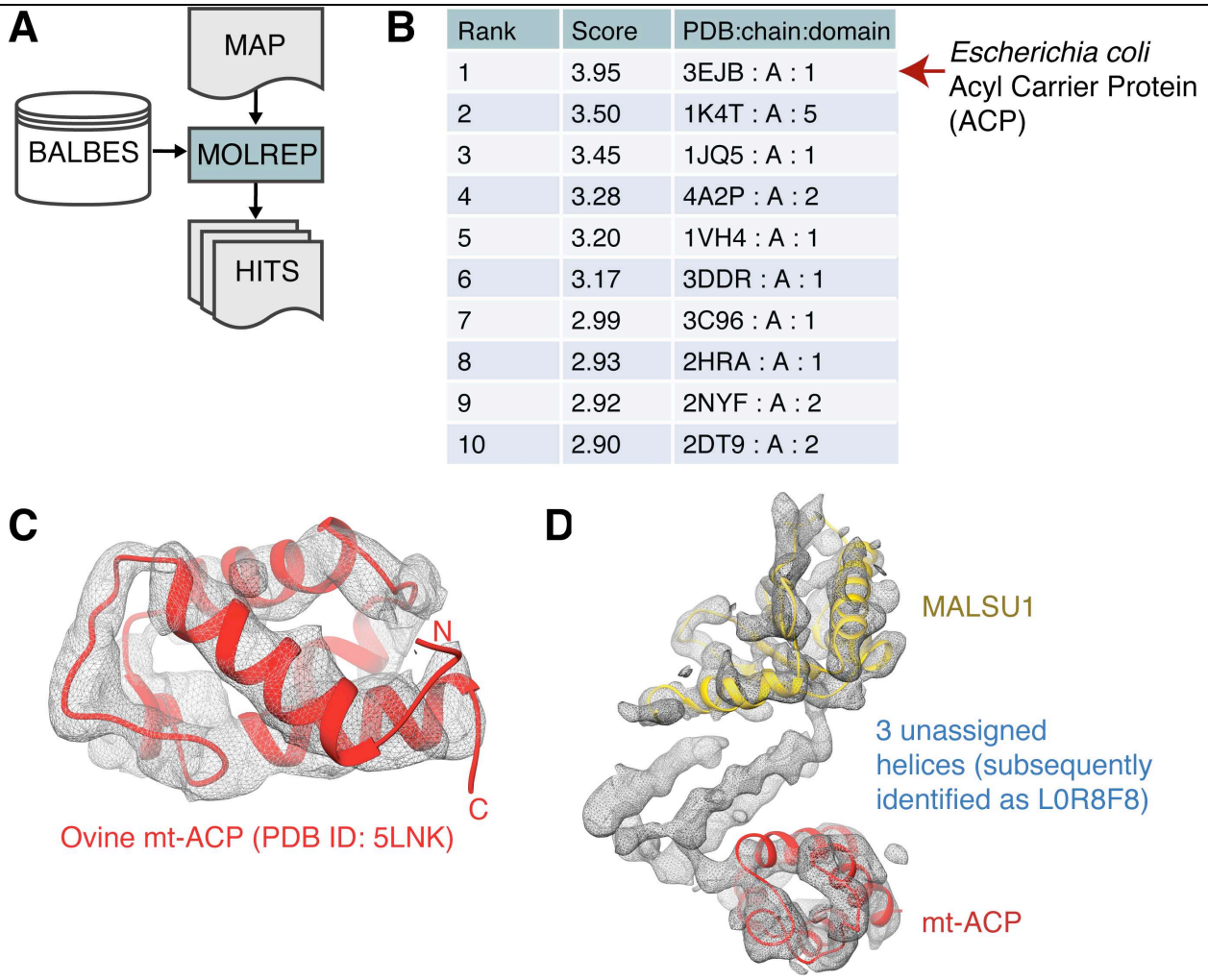

Supplementary Figure 4

Identification of mt-ACP.

(**A**) Schematic of the BALBES-MOLREP pipeline. (**B**) Table of the top ten hits from BALBES-MOLREP, ranked by the contrast score. The top score belongs to ACP from *Escherichia coli*. (**C**) Fit of mammalian mt-ACP to the map. (**D**) Fit of MALSU1 and humanized mt-ACP to the additional density leaves 3 helices unassigned. These helices were subsequently assigned to L0R8F8.

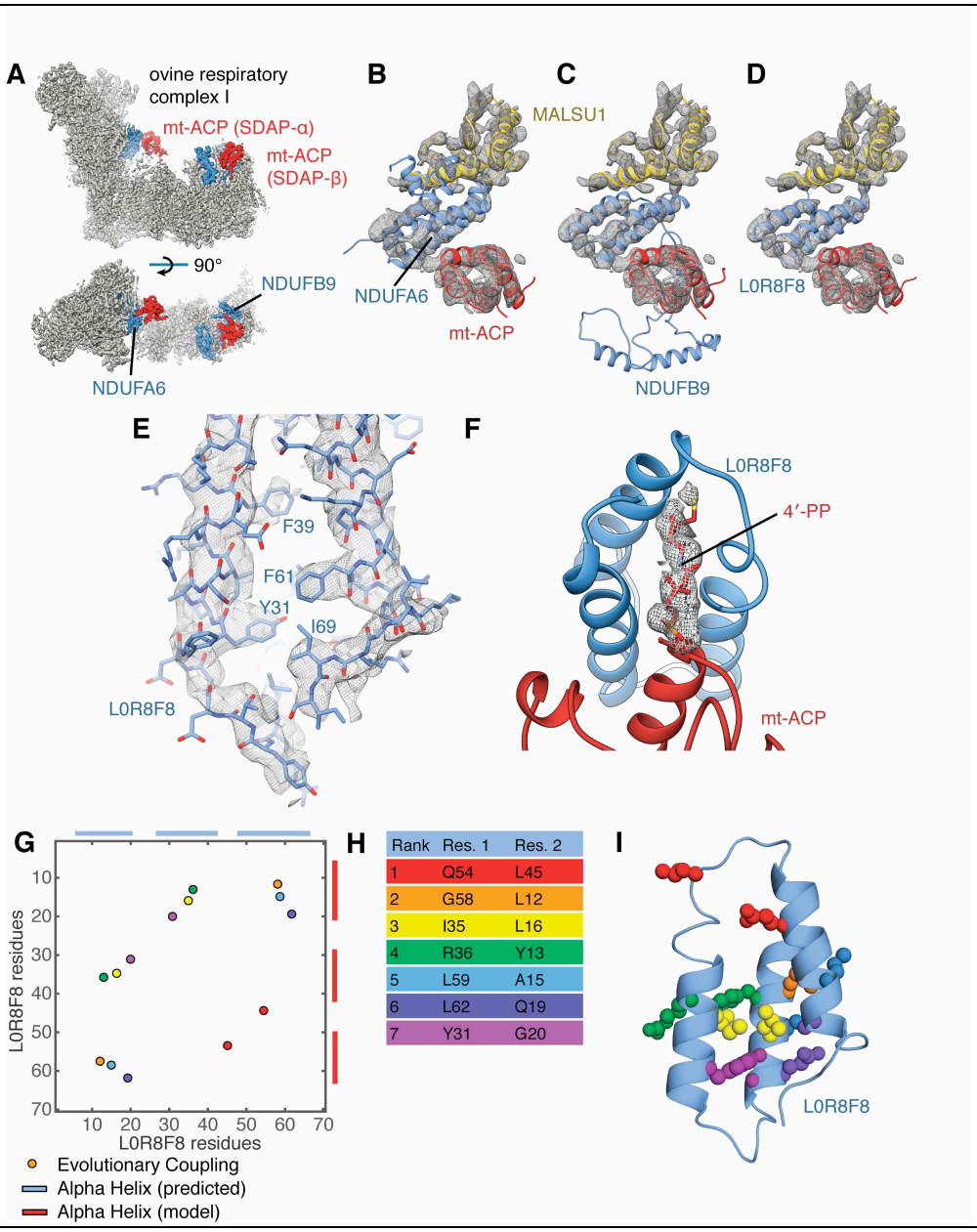

Supplementary Figure 5

Identification of L0R8F8.

(**A**) There are two copies of mt-ACP in mammalian complex I (SDAP-α and SDAP-β), each of which contacts a different LYR-motif protein (NDUFA6 and NDUFB9, respectively). (**B**) Fit of NDUFA6 to the map. (**C**) Fit of NDUFB9 to the map. (**D**) Fit of L0R8F8 to the map. (**E**) Aromatic residues guided the *de novo* modeling of L0R8F8. (**F**) Density present in the core of L0R8F8 corresponds to the 4′-phosphopantetheine (4′-PP) modification of serine 112 of mt-ACP. (**G**) The top seven highest-ranking evolutionary couplings for L0R8F8 plotted as colored dots. The predicted secondary structure closely matches the secondary structure extracted from the model. (**H**) Table of the top seven highest-ranking evolutionary couplings colored according to G. (**I**) Evolutionary couplings mapped onto the structure of L0R8F8. Evolutionary coupled residues are typically in close spatial proximity, as would be expected for a correctly built fold.